

# Simulating quantum light propagation through atomic ensembles using matrix product states

Marco T. Manzoni,<sup>1</sup> Darrick E. Chang,<sup>1</sup> and James S. Douglas<sup>1,\*</sup>

<sup>1</sup>*ICFO-Institut de Ciències Fòniques, The Barcelona Institute of Science and Technology, 08860 Castelldefels (Barcelona), Spain*

(Dated: February 22, 2017)

A powerful method to interface quantum light with matter is to propagate the light through an ensemble of atoms. Recently, a number of such interfaces have emerged, including Rydberg ensembles and atoms coupled to nanophotonic systems, in which strong nonlinear interactions between the propagating photons can be attained. An interesting and largely open problem is whether these systems can produce exotic many-body states of light, as the number of input photons is increased. To gain insight into this problem, it would be highly desirable to find approaches to numerically simulate light propagation in the many-body limit, a goal which has remained elusive thus far. Here, we describe an approach to this problem using a “spin model” that maps a quasi one-dimensional (1D) light propagation problem to the dynamics of an open 1D interacting spin system, where all of the photon correlations are obtained from those of the spins. The spin dynamics in turn can be numerically solved using the toolbox of matrix product states. As a specific example, we apply this formalism to investigate vacuum induced transparency, wherein a pulse propagates with a photon number-dependent group velocity, thereby enabling separation of different photon number components at the output.

Atomic ensembles are a very successful platform used to couple input light to atomic degrees of freedom, allowing the development of new quantum technologies. Historically, the weak optical nonlinearities associated with atomic ensembles have allowed most of the processes of interest, such as quantum memories for light [1], to be describable within a limited realm of classical linear optics or Gaussian quantum states [2]. More recently, it has become possible to engineer strong interactions between photons in atomic ensembles and thereby realize highly non-Gaussian states. Under weak field inputs, for example, phenomena such as photon blockade [3] or two-photon bound states [4] in atomic Rydberg gases [5–7] have been experimentally demonstrated. A number of other systems, such as atoms coupled to nanophotonic waveguides [8–13] or superconducting qubits coupled to transmission lines [14–16] also show potential to realize similar physics.

A major question of interest is what occurs in such systems at higher field inputs. In particular, it is expected that strong interactions might lead to interesting many-body phenomena involving photons, such as photon crystallization (illustrated schematically in Fig. 1(a)). To address this question theoretically seems challenging: the systems are out of equilibrium, being driven by an external laser source; are open, where spontaneous decay of atoms leads to losses; and have long range interactions between atoms mediated by the exchange of photons. Some progress has been made in limiting regimes, where for example effective theories can emerge under certain approximations [11, 12, 17–21]. While these effective theories provide useful insights, it would also be

highly desirable to develop numerical methods with minimal approximations to verify these models and investigate regimes where the approximations break down, potentially revealing new physics as a result.

Currently numerical techniques are quite limited. For example, the standard approach is to model the continuum in which fields propagate by a finite number  $M$  of boxes, as depicted in Fig. 1b, and solving the dynamics of a discretized quantum wave equation [3]. To describe a state with up to  $n$  photons in each box then requires a Hilbert space with dimension of at least  $(n + 1)^M$  (plus any atomic degrees of freedom associated with each box). In practice, this has limited numerical simulations to two [3, 4, 22, 23] or three [20] total excitations over the entire system, and excluding the full effects of dissipation (in particular, either quantum jumps in wave function evolution, or population recycling terms in density matrix evolution). Furthermore, the non-linearity due to atom saturation can typically only be treated effectively, by introducing artificial delta function interactions between the fields. Meanwhile, this discretization of space is clearly inefficient if we consider the trivial example of free space without atoms, where we require a large Hilbert space to propagate a purely photonic wave function.

Motivated by the above observation, it would be natural to devise an alternative numerical approach, whose complexity becomes trivial in the limit of free space. Here, we show that such an approach is possible, by mapping the problem onto the dynamics of a one-dimensional (1D) open “spin” model, which can be solved using the powerful matrix product state ansatz [24, 25] developed in condensed matter physics. The three main steps, which we describe in greater detail below, are:

(i) *Spin model.* In the problem of light propagation through an atomic ensemble, we show that the only inde-

---

\* Corresponding author james.douglas@icfo.eu

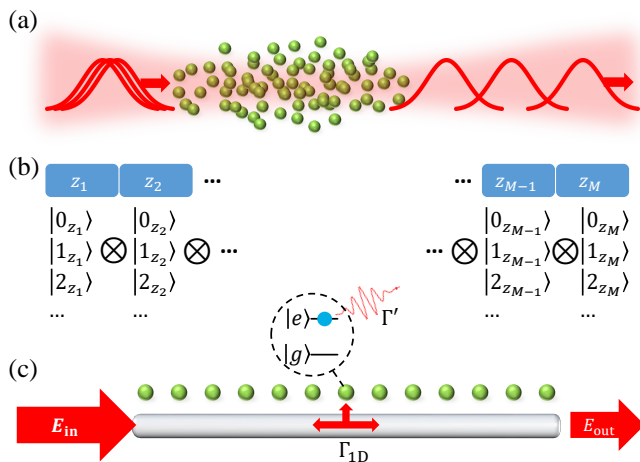


FIG. 1. (a) Light propagation through atomic ensembles with strong inter-atomic interactions can lead the quantum properties of the light to be strongly modified, represented here as crystalline-like output of photons from the medium. (b) In a typical approach to treat such quantum light propagation numerically, space is broken up into  $M$  discrete units centred at positions  $z_j$ , with corresponding local Fock basis states  $|0_{z_j}\rangle, |1_{z_j}\rangle, \dots$  for the photons. The equations of motion for the field may be solved on this space, where the growth of the Hilbert space with the number of Fock components on each site typically restricts such calculations to a maximum of two or three photons in the entire systems. (c) Here instead we model the quasi-1D propagation problem by a 1D waveguide coupled to  $N$  atoms. In this case the degrees of freedom associated with the light field are integrated out, to produce an effective model consisting of an interacting “spin” chain (with the spins being associated with atomic internal states). Output fields are then calculated from the spin dynamics using an input-output relation. The Hilbert space required to treat the problem is then determined by the number of atoms and propagation in free space absent atoms becomes trivial. As discussed in Section II the atoms are coupled to the waveguide modes with strength  $\Gamma_{1D}$  and for the simple case of two-level atoms the excited state  $|e\rangle$  may also decay into modes outside of the waveguide at rate  $\Gamma'$ .

pendent degrees of freedom are the atomic internal states (“spins”). In particular, the fields mediate interactions between the atoms and can be integrated out, reducing the description to a problem of  $N$  interacting spins. The process of integrating out the field results in a generalized “input-output” relation, which formally relates the outgoing quantum field to the input field and correlation functions of the spins [26–29]. By treating the problem from the atomic point of view, the saturation of atoms is explicitly included and the limit of free space (absent atoms) is numerically trivial.

(ii) *Waveguide model.* Many light propagation experiments are quasi-one dimensional, where the input light is in a single transverse mode and the output is measured in the same mode. Scattering out of this mode leads to dissipation. In this case, a simpler model of the propagation problem that captures the same physics is a one-

dimensional waveguide coupled to an ensemble of atoms as shown in Fig. 1(c). Furthermore, in known problems of interest, the atom number does not appear independently, but rather macroscopic observables such as optical depth depend on the product of atom number and single-photon, single-atom interaction probability. By tuning this probability to be large in the waveguide, a relatively small ( $\sim 10^2$ ) number of atoms is sufficient to model atomic ensemble experiments thus far. Moreover, this 1D model also captures quantitatively well actual systems where atoms and qubits are coupled to waveguides [13, 30].

(iii) *Solution with MPS.* The spin model description allows one to borrow from the extensive toolbox developed in condensed matter physics for treating spin systems. Here we apply the powerful technique of matrix product states (MPS) [24, 25] to numerically simulate the system. This technique depends on the fact that many of the quantum states we encounter in reality do not have large amounts of entanglement and are confined to a small portion of the in-principle exponential Hilbert space, allowing for a more efficient state ansatz. While the amount of entanglement present in atom-light interfaces is a generally unstudied problem, we give heuristic arguments below why we expect the MPS ansatz to work for such systems. We also quantitatively confirm the convergence of our numerics versus increasing size of the MPS.

To benchmark this model we apply it to simulate pulse propagation in the case of vacuum induced transparency [31, 32], which is one of the few cases where many-photon propagation is qualitatively understood [23, 33]. Specifically, the effect relies on taking a traditional setup for electromagnetically induced transparency [1] where the group velocity of a probe field is dictated by a large classical control field, and replacing that control field with the vacuum Rabi interaction provided by an optical cavity. In that case, the light propagation acquires non-linearity from the cavity-atom coupling, and the velocity of propagation of the probe field depends directly on its photon number. For an input pulse that is a superposition of different number states, such as a coherent state, the different number components then become spatially separated at output.

## I. SPIN MODEL OF LIGHT PROPAGATION

We wish to solve for the coupled dynamics of a quantum field  $\mathbf{E}(\mathbf{r}, t)$  as it propagates through and interacts with an ensemble of atoms. For concreteness, we will assume that the field couples to a single dipole-allowed transition from atomic ground state  $|g\rangle$  to excited state  $|e\rangle$ , although the following derivation can readily be generalized to more complicated level structure. Numerically, to keep track of the field explicitly is difficult due to its continuous nature. However, the problem can be simplified considerably by recognizing that the proper-

ties of the field are completely determined by the atoms, as is described in Refs. [26, 29], the results of which we summarize here. Key to this approach is a field quantization scheme based upon the (classical) electromagnetic Green's function [29, 34, 35]. Formally, the Green's function is the solution to

$$\left[ (\nabla \times \nabla \times) - \frac{\omega^2}{c^2} \epsilon(\mathbf{r}, \omega) \right] \mathbf{G}(\mathbf{r}, \mathbf{r}', \omega) = \delta(\mathbf{r} - \mathbf{r}') \mathbb{I}, \quad (1)$$

where  $\epsilon(\mathbf{r}, \omega)$  describes the relative permittivity of the medium in which the light is propagating in absence of the atoms. Physically, the Green's function describes the field at position  $\mathbf{r}$ , due to a normalized dipole at  $\mathbf{r}'$  oscillating with frequency  $\omega$ .  $G_{ab}$  (with  $a, b = x, y, z$ ) is a tensor quantity, giving the field projected along  $a$  ( $a = x, y, z$ ), due to a source whose dipole moment is oriented along  $b$ .

We can use the Green's function to find the field at any point. Specifically, the atoms act as sources for the field with frequency  $\omega_{eg}$ , which then propagates according to the Green's function. The total field at  $\mathbf{r}$  at any time is then just the sum of this contribution and the input quantum field  $\mathbf{E}_{\text{in}}(\mathbf{r}, t)$ . In total we have

$$\mathbf{E}(\mathbf{r}, t) = \mathbf{E}_{\text{in}}(\mathbf{r}, t) + \mu_0 \omega_{eg}^2 \sum_{j=1}^N \mathbf{G}(\mathbf{r}, \mathbf{r}_j, \omega_{eg}) \cdot \mathbf{d} \sigma_{ge}^j, \quad (2)$$

where  $\mathbf{d}$  is the dipole moment associated with the transition  $|e\rangle - |g\rangle$ . Similar equations appear often in the case of classical fields and dipoles, and simply state that the total field consists of the incident field plus that radiated by the dipoles. In the case where the field and dipoles are quantum operators, this equation remains true, as the classical and quantum fields obey the same wave equation.

In the Heisenberg equations of motion for the atomic degrees of freedom, an atom at position  $\mathbf{r}$  is driven by the total field  $\mathbf{E}(\mathbf{r}, t)$  at the same point. However, from Eq. (2), one sees that the resulting dynamics can be formulated purely in terms of atoms interacting with an input field, and atoms interacting with one another. Part of the inter-atomic interactions can be derived from a Hermitian Hamiltonian,

$$H_{\text{dd}} = -\mu_0 \omega_{eg}^2 \sum_{j,l=1}^N \mathbf{d}^* \cdot \text{Re}\{\mathbf{G}(\mathbf{r}_j, \mathbf{r}_l, \omega_{eg})\} \cdot \mathbf{d} \sigma_{eg}^j \sigma_{ge}^l. \quad (3)$$

This Hamiltonian describes the process of emission by an excited atom at  $\mathbf{r}_j$ , and the subsequent absorption of that photon by a ground-state atom at  $\mathbf{r}_l$ . The remaining inter-atomic dynamics can be derived from a master equation, which physically describes the processes of individual or collective spontaneous emission,

$$\mathcal{L}_{\text{dd}}[\rho] = \sum_{j,l=1}^N \frac{\Gamma_{j,l}}{2} (2\sigma_{ge}^j \rho \sigma_{eg}^l - \sigma_{eg}^j \sigma_{ge}^l \rho - \rho \sigma_{eg}^j \sigma_{ge}^l), \quad (4)$$

where  $\Gamma_{j,l} = 2\mu_0 \omega_{eg}^2 \mathbf{d}^* \cdot \text{Im}\{\mathbf{G}(\mathbf{r}_j, \mathbf{r}_l, \omega_{eg})\} \cdot \mathbf{d}$ .

It remains to treat the driving of the atoms by the input field, where in the following we will be interested in the case of a coherent state input. In that case, the effect on the atoms is captured by the Hamiltonian [36]

$$H_{\text{drive}} = - \sum_{j=1}^N (\mathcal{E}_{\text{in}}(\mathbf{r}_j, t) \sigma_{eg}^j + \text{H.c.})/2, \quad (5)$$

where  $\mathcal{E}_{\text{in}}(\mathbf{r}_j, t)$  is the Rabi frequency associated with the input probe.

## II. ONE DIMENSIONAL WAVEGUIDE

The dynamics of the full system are now reduced to following the atomic evolution generated by the above equations with the addition of any arbitrary atomic evolution described by  $H_0$ , which could for example describe Rydberg interactions between atoms or multilevel atoms driven by external classical fields. In particular, in the case of  $N$  two-level systems, the Hilbert space has been reduced to a finite size of  $2^N$ . However, many experiments of interest take place in optically dense media, where  $N \sim 10^6$ , which thus still makes direct numerical implementation intractable. There are indeed some phenomena involving atomic ensembles that are truly three-dimensional and involve a large number of atoms, such as radiation trapping [37] and other phenomena associated with high densities [38, 39]. However, within the context of generating many-body states of light, the problems of interest thus far involve quasi one-dimensional propagation, where the light is input in a single transverse mode and the output is taken from the same mode. Thus, the corresponding wave equation is taken to be one-dimensional [2–4, 40]. We may then model such a system by a chain of atoms coupled to a true one-dimensional waveguide. The advantage of this approach, which we detail further below, is that one can reproduce macroscopic observables of a free-space system using a much smaller number of atoms, by an appropriate choice of parameters for the 1D system.

Reducing the system to one dimension simplifies Eqs. (3)-(4), where the Green's function propagation gives simply a phase factor corresponding to the distance between the atoms  $G(z, z', \omega_{eg}) \sim i \exp(ik_0|z - z'|)$ , for  $k_0 = \omega_{eg}/c$ . The waveguide mediated dipole-dipole interactions and the dissipation are then given by [41]

$$H_{\text{dd}} = \frac{\Gamma_{1\text{D}}}{2} \sum_{j,l=1}^N \sin(k_0|z_j - z_l|) \sigma_{eg}^j \sigma_{ge}^l, \quad (6)$$

and

$$\begin{aligned} \mathcal{L}_{\text{dd}}[\rho] = & -\frac{\Gamma_{1\text{D}}}{2} \sum_{j,l=1}^N \cos(k_0|z_j - z_l|) \\ & \times (2\sigma_{ge}^j \rho \sigma_{eg}^l - \sigma_{eg}^j \sigma_{ge}^l \rho - \rho \sigma_{eg}^j \sigma_{ge}^l), \end{aligned} \quad (7)$$

where  $\Gamma_{1D}$  is the decay rate of a single excited atom into the guided modes of the waveguide, propagating left and right. In addition, we can add an phenomenological independent decay rate  $\Gamma'$  for excited atoms into channels other than the waveguide, which in our mapping from a 3D atomic ensemble corresponds to scattering out of the quasi-1D input mode. This is described by the locally acting Lindblad operator  $\mathcal{L}_{\text{spont}}[\rho] = -\frac{\Gamma'}{2} \sum_{j=1}^N (2\sigma_{ge}^j \rho \sigma_{eg}^j - \sigma_{eg}^j \sigma_{ge}^j \rho - \rho \sigma_{eg}^j \sigma_{ge}^j)$ . The coupling with the input field, assumed to be right-propagating, is given by  $H_{\text{drive}} = \sqrt{\Gamma_{1D}/2} (\mathcal{E}_{\text{in}}(t) e^{iz_j k_0} \sigma_{eg}^j + \text{H.c.})$ . Along with this we have the output field, measured at the right end of the atomic medium  $z_{\text{end}}$ , which is given by

$$E_{\text{out}}(t) = \mathcal{E}_{\text{in}}(z_{\text{end}}, t) - i\sqrt{\Gamma_{1D}/2} \sum_j e^{ik_0(z_{\text{end}} - z_j)} \sigma_{ge}^j. \quad (8)$$

Here we have neglected an additional quantum noise term associated with the input field,  $\epsilon_{\text{in}}(t)$ , as this does not contribute to the normally ordered correlation functions of the output field that we will be interested in.

The coupling of the atoms to the waveguide and the positions of the atoms must be chosen carefully to reproduce phenomena associated with free-space ensembles. In particular, as we discuss below, our numerical calculations are facilitated by choosing ratios of  $\Gamma_{1D}/\Gamma' \sim 1$ . It is known that for a weak resonant input field, a single two-level atom can produce an appreciable reflectance of  $\Gamma_{1D}^2/(\Gamma_{1D} + \Gamma')^2$  [42, 43]. The reflectance can be further enhanced if multiple atoms are placed on a lattice with lattice constant defined by  $k_0 a = \pi$ , in which case the reflectance from individual atoms constructively interferes [41, 44, 45]. While it is possible to observe similar effects in atomic ensembles [46, 47], this situation is atypical and will not be discussed further here. To reproduce the typical case in atomic ensembles where reflection is negligible, we choose a spacing  $k_0 a = \pi/2$ , in which reflection from different atoms in the lattice destructively interferes.

In this configuration, the 1D waveguide model reproduces one of the key features of an atomic ensemble, that of decay of the transmitted field with increasing optical depth. If we consider the transmittance  $T = \langle E_{\text{out}}^\dagger E_{\text{out}} \rangle / |\mathcal{E}_{\text{in}}|^2$ , then for a resonant weak coherent state input we find in the 1D waveguide model  $T = \exp(-\text{OD})$ , where the optical depth is  $\text{OD} = 2N\Gamma_{1D}/\Gamma'$  for  $\Gamma_{1D} \lesssim \Gamma'$  [12]. Since  $\text{OD} \lesssim 10^2$  in realistic atomic ensembles, by artificially choosing  $\Gamma_{1D} \sim \Gamma$ , the same optical depth is achieved with just tens or hundreds of atoms. While our 1D model reproduces the macroscopic observables of light propagation in a traditional atomic ensemble, we note that it also quantitatively captures the microscopic details of experiments where atoms or other quantum emitters are coupled to 1D channels. This includes atoms coupled to nano-fibers ( $\Gamma_{1D}/\Gamma' \sim 0.05$ ) [13] or photonic crystals ( $\Gamma_{1D}/\Gamma' \sim 1$ ) [30], or “artificial” atoms such as superconducting qubits or quantum dots coupled to waveguides ( $\Gamma_{1D}/\Gamma' \gg 1$ ) [14–16, 48].

To find the time dynamics for the spin model we must evolve the master equation in time. Numerically this can be done directly by evolving the full density matrix  $\rho$  in time using standard techniques such as the Runge-Kutta algorithm. Alternatively, we can instead use the “quantum jump” approach to unravel the master equation into trajectories of evolving pure states [49, 50]. Such an approach is helpful when the size of the density matrix ( $d^N \times d^N$ , with  $d$  being the Hilbert space dimension of a single atom) becomes too large, even if the size of the wave function ( $d^N$ ) in the Hilbert space remains tractable.

Here, we briefly review the quantum jump formalism, so that the implementation with MPS described later will be more clear. We write the master equation for our 1D spin model in the form  $\dot{\rho} = -i(H_{\text{eff}}\rho - \rho H_{\text{eff}}^\dagger) + \sum_l O_l \rho O_l^\dagger$ , where  $O_l$  are the “jump” operators associated with the dissipation resulting from emission into the waveguide and into free space, and  $H_{\text{eff}}$  is a non-Hermitian effective Hamiltonian. This division of the master equation into jump terms and an effective Hamiltonian  $H_{\text{eff}}$  is not unique and we attempt to do so here in a way that the jump operators have a physical significance. In particular, the emission of a photon into the right going mode of the waveguide may interfere with the input light that is also travelling to the right (see Eq. (8)), an interference that would be present in real detection of photons output from the waveguide. This interference can be taken into account in our jump operator, and as such we take the right going jump operator to be  $O_R = \mathcal{E}_{\text{in}}(t) - i\sqrt{\Gamma_{1D}/2} \sum_j e^{-ik_0 z_j} \sigma_{ge}^j$  (in contrast with  $O_R = \sqrt{\Gamma_{1D}/2} \sum_j e^{-ik_0 z_j} \sigma_{ge}^j$  as in Ref. [26]). The left going jump operator is simpler given the lack of input field in that mode,  $O_L = \sqrt{\Gamma_{1D}/2} \sum_j e^{ik_0 z_j} \sigma_{ge}^j$ . In addition, we have  $N$  local jump operators  $O_j = \sqrt{\Gamma'} \sigma_{ge}^j$  corresponding to the free space decay, giving a set of possible jumps  $O_l \in \{O_R, O_L, O_1, \dots, O_N\}$ . With the jumps formulated in this way the effective Hamiltonian becomes

$$H_{\text{eff}} = H_0 - i\frac{\Gamma_{1D}}{2} \sum_{j,l=1}^N \exp(ik_0|z_j - z_l|) \sigma_{eg}^j \sigma_{ge}^l - \sqrt{\frac{\Gamma_{1D}}{2}} \mathcal{E}_{\text{in}}(t) \sum_j e^{-ik_0 z_j} \sigma_{eg}^j - \frac{i}{2} |\mathcal{E}_{\text{in}}(t)|^2. \quad (9)$$

In general  $H_0$  can describe any additional atomic evolution; in the specific case of two level atoms coupled to a probe of frequency  $\omega_p$  we can write, in the frame rotating with in the input frequency,  $H_0 = \sum_j (-\Delta - i\Gamma'/2) \sigma_{ee}^j$ , where  $\Delta = \omega_p - \omega_{eg}$ .

The quantum jump approach uses the above decomposition of the master equation to restate the evolution of the density operator as a sum of pure state evolutions called trajectories [49], where the wave function evolution is divided into (a) deterministic evolution under  $H_{\text{eff}}$  and (b) stochastic quantum jumps made by applying jump operators  $O_l$ . Starting from a pure state

$|\psi(t)\rangle$  at time  $t$ , the deterministic evolution over a time step  $\delta t$  gives  $|\psi(t + \delta t)\rangle = e^{-iH_{\text{eff}}\delta t} |\psi(t)\rangle$ . However, during this evolution the norm of the state decreases to  $\delta p = 1 - \langle \psi(t) | e^{iH_{\text{eff}}^\dagger \delta t} e^{-iH_{\text{eff}} \delta t} | \psi(t) \rangle$ , as the effect of the jump operators is neglected. The effect of these operators is instead accounted for stochastically, where after each deterministic evolution we generate a random number  $r$  between 0 and 1. If  $r > \delta p$  the system remains in state  $|\psi(t + \delta t)\rangle$ . Otherwise, the state makes a random quantum jump to  $|\psi(t + \delta t)\rangle = O_l |\psi(t)\rangle$  with probability  $\delta p_l = \delta t \langle \psi(t) | O_l^\dagger O_l | \psi(t) \rangle$ . The state is then normalized and the process repeats for the next time step and each sequence of evolutions gives a quantum trajectory. Any observable can be obtained by averaging its value over many trajectories. Furthermore, as we choose our quantum jumps to relate to physical processes, the distribution of the jumps can be thought of as corresponding to actual photon detection in an experiment.

### III. SIMULATIONS USING MATRIX PRODUCT STATES

Using the 1D spin model described above significantly reduces the size of the Hilbert space required to simulate the light propagation problem, but the dimension still grows exponentially with atom number. This growth can be avoided in the case where the input field is sufficiently weak that the Hilbert space can be truncated to a maximum number of total excitations likely to be found in the system [12, 26]. In the more general case, where many-photon effects are important, the full Hilbert space may be treated numerically for around 10 to 20 atoms depending on the size of the single-atom Hilbert space dimension  $d$ . Going beyond this requires some reduction of the Hilbert space and here we choose to use matrix product states (MPS), which have been successfully used in condensed matter to model a wide variety of 1D interacting spin systems [24, 25].

The key idea behind MPS is to represent the quantum state of the spin chain in a local representation where only a tractable number of basis states from the full Hilbert space is retained. In the case of time evolution, these basis states are updated dynamically in order to have optimum overlap with the true state wave function. In particular, the wave function of a many-body system  $|\psi\rangle = \psi_{\sigma_1, \sigma_2, \dots, \sigma_N} |\sigma_1, \sigma_2, \dots, \sigma_N\rangle$  can be represented by reshaping the  $N$ -dimensional tensor  $\psi_{\sigma_1, \sigma_2, \dots, \sigma_N}$  into a matrix product state of the form

$$|\psi\rangle_{\text{MPS}} = \sum_{\sigma_1, \dots, \sigma_N} A^{\sigma_1} A^{\sigma_2} \dots A^{\sigma_N} |\sigma_1, \sigma_2, \dots, \sigma_N\rangle, \quad (10)$$

where  $\sigma_j$  represent the local  $d$ -dimensional Hilbert space of the atoms, *e.g.*,  $\sigma_j \in \{|e\rangle, |g\rangle\}$  for two-level atoms. Each site  $j$  in the spin chain has a corresponding set of  $d$  matrices,  $A^{\sigma_j}$ , and by taking the product of these matrices for some combination of  $\sigma_j$ 's we then recover

the coefficient  $\psi_{\sigma_1, \sigma_2, \dots, \sigma_N}$ . The matrices have dimensions  $D_{j-1} \times D_j$  for the  $j$ th site ( $D_0 = D_{N+1} = 1$ ), which are referred to as the bond dimensions of each matrix. We also define  $D = \max_j D_j$  as the maximum bond dimension of the state  $|\psi\rangle_{\text{MPS}}$ . This representation is completely general, and as such the bond dimensions grow exponentially in size for arbitrary quantum states. In certain circumstances, however, the bond dimension  $D$  needed to approximate a state well might grow more slowly with  $N$ , which enables MPS to serve as an efficient representation.

For example, this forms the underlying reason for the efficiency of density-matrix renormalization group algorithms for computing ground states of 1D systems with short-range interactions [51]. A priori, for our system involving the dynamics of an open system with long-range interactions, we know of no previous work that makes definitive statements about the scaling of  $D$ . We can provide some intuitive arguments, however, that MPS should work well (at least without additional interactions added to the system). First, we note that although the dipole-dipole interaction term in Eq. (9) appears peculiar, being infinite-range and non-uniform, it conserves excitation number. For a single excitation, it simply encodes a (well-behaved) linear optical dispersion relation that propagates a pulse from one end of the atomic system to the other [12]. While the spin nature in principle makes the atoms nonlinear, thus far in atomic ensemble experiments the strength of nonlinearity arising purely from atomic saturation remains very small at the level of single photons, and thus one can hypothesize that only a small portion of the Hilbert space is explored.

We next describe how to implement the quantum jump dynamics within the MPS wave function description [50, 52]. As an aside, however, we note that MPS-based techniques for evolution of density matrices have also been developed [53–56]. Whether and when such techniques out-perform quantum jump methods for our problem is likely a subtle question, which will be explored in more detail in future work.

There are four essential manipulations of the MPS as illustrated in Fig. 2. Analogous to our description of the quantum jump algorithm in Section II, we first describe how to implement (a) deterministic evolution over a small discrete time step  $\delta t$ , and (b) stochastic quantum jumps that account for dissipation. Additional steps specific to MPS are (c) state compression, to constrain the growth of the MPS representation of the state in time, and (d) calculation of observables such as the output field given an MPS representation of a state.

(a) *Time evolution.* To evolve the state  $|\psi(t)\rangle$  in time we need to apply the operator  $e^{-iH_{\text{eff}}\delta t}$  to the MPS representation. This is achieved by applying a matrix product operator (MPO) to the state, where just as a state can be decomposed into an MPS, any operator  $W$  can be

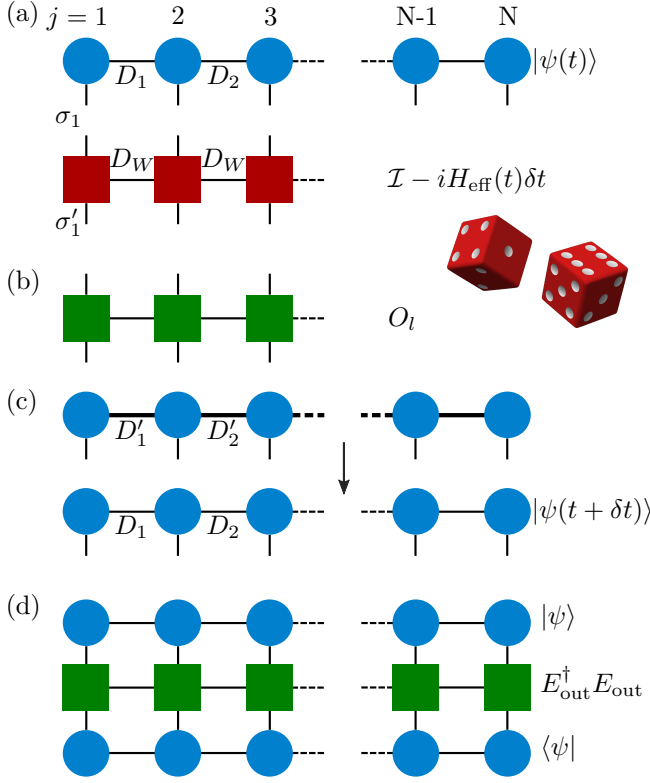


FIG. 2. Schematic of MPS operations (a) Deterministic time evolution of MPS. The initial state  $|\psi(t)\rangle$  in MPS form is presented pictorially as a tensor network, where the circles represent the set of local matrices  $A^{\sigma_j}$  on each site  $j$ . The lines or bonds joining the circles represent the contraction of these local tensors to give the state  $|\psi(t)\rangle$ , where the bonds have dimension  $D_j$ . The open ended lines correspond to the local  $d$ -dimensional Hilbert space of the atoms  $\sigma_j$ . The deterministic evolution is then found by contracting these open connectors with those of the MPO representing  $e^{-iH_{\text{eff}}\delta t} \approx 1 - iH_{\text{eff}}\delta t$ , which is represented here by the tensor network of red squares. (b) Quantum jumps. After each deterministic evolution a random number generator is used to decide whether quantum jumps should be applied to the wave function. This is achieved by applying the MPO corresponding to a quantum jump  $O_l$  represented here by a tensor network of green squares. (c) After the application of the time evolution or jump MPOs the resulting MPS has larger bond dimension, e.g.,  $D_1' = D_W \times D_1$ , and is compressed, typically back to the original bond dimension, although this can be increased if the compression produces a large error. (d) Measurement of observables. At any time we may measure an observable by sandwiching the corresponding MPO, here for example  $E_{\text{out}}^\dagger E_{\text{out}}$ , between the MPS representing  $|\psi\rangle$  and  $\langle\psi|$ , so that the corresponding tensor contraction yields  $\langle\psi| E_{\text{out}}^\dagger E_{\text{out}} |\psi\rangle$ .

expressed in a local representation as

$$W = \sum_{\sigma'_1, \dots, \sigma'_N, \sigma_1, \dots, \sigma_N} W^{\sigma'_1, \sigma_1} W^{\sigma'_2, \sigma_2} \dots W^{\sigma'_N, \sigma_N} \times |\sigma'_1, \sigma'_2, \dots, \sigma'_N\rangle \langle\sigma_1, \sigma_2, \dots, \sigma_N|. \quad (11)$$

Here  $W^{\sigma'_j, \sigma_j}$  are a set of matrices at site  $j$ , where the matrices now have two physical indices  $\sigma'_j, \sigma_j$  due to  $W$  being an operator. An MPO may be “applied” to an MPS via a tensor contraction over the physical indices  $\sigma_j$  of the MPS and MPO, as shown in Fig. 2(a). This generates a new MPS with higher bond dimension, as the bond dimension of the MPO,  $D_W$ , multiplies the bond dimension of the original MPS, and for the calculation to be tractable  $D_W$  must be small. Such a compact form is not known for the operator  $e^{-iH_{\text{eff}}\delta t}$ ; however, the first order approximation  $e^{-iH_{\text{eff}}\delta t} = 1 - iH_{\text{eff}}\delta t$  has a compact MPO form if  $H_{\text{eff}}$  does. This is the case for the 1D spin model where the bond dimension is  $D_W = 4$ , see Appendix A. Using a small time step  $\delta t$  we can then advance the wave function in time.

(b) *Quantum jumps.* After evolving a time  $\delta t$ , the state is either kept and renormalized, or a jump is applied, as described in Section II. To apply the quantum jump formalism we then just require an MPO form of the jump operators that can be applied to the MPS at each time step, see Fig. 2(b). The jump operators of the 1D spin model can be written in compact MPO form, where the loss into free space is a local matrix operation, and loss into the waveguide requires an MPO of bond dimension  $D_W = 2$ , as described in Appendix A.

(c) *State compression.* After applying the time evolution operator or jump operators the size of the MPS increases as the bond dimension of the operator multiplies the bond dimension of the original state. Over time this would lead to exponential growth in the MPS size if not constrained. This increase in bond dimension can correspond to the true build up of entanglement, but may also correspond to the new state being expressed inefficiently in the MPS form. In the second case, a more efficient representation can be found and the bond dimension compressed to a smaller value, as in Fig. 2(c). This can be done using singular value decompositions to find low rank approximations of the matrices  $A^{\sigma_j}$  in the MPS representation, or by variationally exploring the space of MPS states with a fixed bond dimension that are closest to the original state [24, 25]. The validity of such a compression can be evaluated by checking how strongly the parts of the state discarded in the compression contribute to the description. From this an error can be calculated and the bond dimension in the compression adjusted so the error remains small, see Appendix B.

(d) *Calculating observables.* At any point in time observables such as the spin populations or output field may be calculated for a particular quantum trajectory by applying the appropriate operator associated with that observable in MPO form to the state. For example, to find the output intensity,  $\langle\psi(t)| E_{\text{out}}^\dagger(t) E_{\text{out}}(t) |\psi(t)\rangle$ , one can express the individual elements as matrix product states or operators. The intensity for that trajectory can then be evaluated through a tensor contraction, as shown in Fig. 2(d). This intensity is then averaged over all the quantum trajectories to find the expectation value  $I_{\text{out}}(t) = \langle E_{\text{out}}^\dagger(t) E_{\text{out}}(t) \rangle$ . Multi-time correlation func-



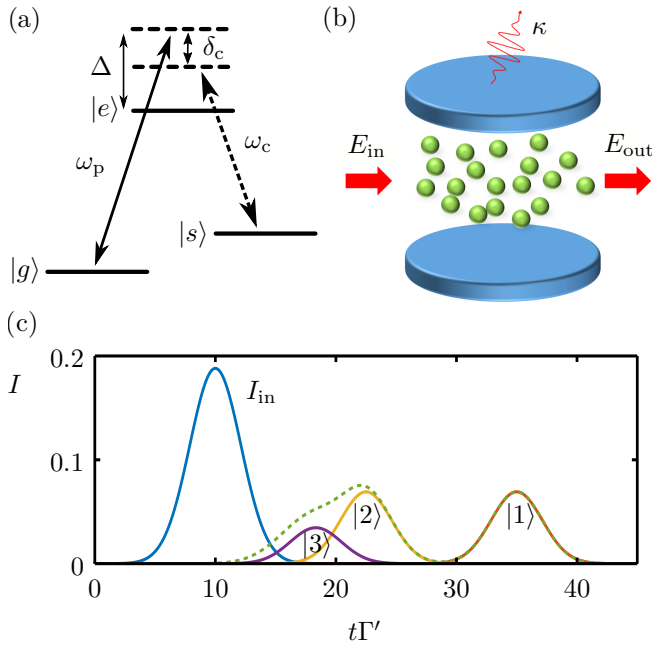


FIG. 3. (a) Three-level atoms, where the transition  $|s\rangle - |e\rangle$  is coupled to a control or a cavity field with frequency  $\omega_c$ , allow for transparent propagation of probe photons ( $\omega_p$ ) in EIT or VIT. (b) Schematic representation of the VIT setup. An atomic ensemble is trapped inside an optical cavity where the atoms couple both to the probe field  $E_{\text{in}}$  and to a cavity mode which is initially in its vacuum state. Photons in the cavity have an associated decay rate  $\kappa$  from transmission through the mirrors. (c) Idealized time-dependent transmission of a coherent pulse with average number of photons equal to one through a VIT medium. In the case where all loss mechanisms are ignored, as well as the effect of pulse distortion on entry and exit from the atomic ensemble, the individual Fock number state components  $|n\rangle$  of the input pulse (blue) propagate through the medium with group velocity  $v_n \propto n$ . This leads to separation of the one- (red), two- (yellow) and three-photon (violet) components of the output field, and a total output intensity shown by the green dashed line. We have taken  $v_1 = 4a\Gamma'$  and the medium has a length  $L = 100a$ .

tions such as  $I_{\text{out}}^{(2)}(t, t + \tau) = \langle E_{\text{out}}^\dagger(t) E_{\text{out}}^\dagger(t + \tau) E_{\text{out}}(t + \tau) E_{\text{out}}(t) \rangle$  can also be found. This is done by propagating the state in time until time  $t$  and then applying the operator  $E_{\text{out}}$  to the state. The state is evolved a further time  $\tau$  and the operator applied again. The norm of the resulting states are then averaged over many such evolutions to find the two-time correlation.

#### IV. VACUUM INDUCED TRANSPARENCY

The model introduced in the previous sections gives a powerful and flexible algorithm for simulating the interaction of light with atomic ensembles in the multiphoton limit. To demonstrate the utility of this approach we now investigate the phenomenon of vacuum induced

transparency (VIT) [31]. This example also serves to benchmark our method, as exact solutions for non-trivial multiphoton behavior are not available, while in the case of VIT at least the qualitative nature of the system dynamics is understood.

VIT is closely related to the effect of electromagnetically induced transparency (EIT) [1], which occurs in three-level atomic medium. In a two-level medium incoming probe light that couples resonantly to an atomic transition  $|g\rangle - |e\rangle$  is absorbed and scattered by the atoms into other directions, leading for example to the strong attenuation in the linear transmittance for high optical depth,  $T = \exp(-\text{OD})$  (see Section II). In EIT, an additional metastable level  $|s\rangle$  (Fig. 3(a)) is also coupled to the excited state by a classical control field with Rabi frequency  $\Omega$ , allowing probe photons to couple with spin-wave excitations from state  $|g\rangle$  to  $|s\rangle$ , forming so-called “dark-state polaritons.” The coupling to the spin wave leads to a strongly reduced group velocity relative to free space ( $v_g = \Omega^2 a / (2\Gamma_{1D})$  in a waveguide [12]), while the absence of population in  $|e\rangle$  enables a pulse to propagate with minimal attenuation.

In VIT the control field is replaced by strong coupling of the atoms to a resonant cavity mode as shown in Fig. 3(b) [31, 57], which is described by  $g \sum_j (\sigma_{es}^j a + \text{h.c.})$  in the case of uniform coupling  $g$  to a cavity mode with annihilation operator  $a$ . Here even when the cavity is empty the atomic medium can become transparent as vacuum Rabi oscillations transfer population from state  $|e\rangle$  to  $|s\rangle$  [32]. The propagation of light in the system then takes on the nature of the non-linear coupling of the atoms to the cavity. Specifically, the formation of a spin wave from  $n$  probe photons is accompanied by the excitation of the same number of cavity photons, which produce an effective control field strength of  $\sqrt{n}g$ . Since in EIT the group velocity of the light is determined by the control field, where  $v_g \propto |\Omega|^2$ , the group velocity in VIT becomes number dependent  $v_n \sim 2n|g|^2/\Gamma_{1D}$  [23, 33]. Fock states  $|n\rangle$  input into the system are then expected to propagate at  $v_n$ .

On the other hand, a coherent state  $|\alpha\rangle$  that has average number of photons  $|\alpha|^2$  is a superposition of Fock states, where  $n$  photons are present with probability  $e^{-|\alpha|^2} |\alpha|^{2n} / n!$ . Input into the VIT medium, these components are then expected to spatially separate due to their different propagation velocities, with sufficient optical depth. The output intensity can then be calculated naively by simply delaying the input Fock components by a time  $\tau_n = L/v_n$ , where  $L$  is the length of the atomic medium. The output intensity in time resulting from such a toy model is shown in Fig. 3(c), for a coherent state input pulse with average number  $\langle n_{\text{pulse}} \rangle = 1$ . We have taken the system length to be  $L = 100a$  and the single photon velocity  $v_1 = 4a\Gamma'$ , which results for example from taking  $g = 2\Gamma'$  and  $\Gamma_{1D} = 2\Gamma'$  in which case the system’s optical depth is 400. We note that the experimental conditions needed to observe photon number separation in VIT are difficult to achieve [32], and thus

our parameters are chosen to observe the desired effect, rather than correspond to a given experiment.

A plot similar to Fig. 3(c) was given in the original theory of VIT [33], as at that time it was unknown how to calculate observables in the presence of losses and spatio-temporal effects, such as occurring from pulse entry and exit from the atomic medium. More recently, VIT has also been studied numerically in the weak-field limit using the space discretization technique schematically illustrated in Fig. 1(b) [23]. In the weak field limit, only the single photon manifold contributes to the output intensity and the higher number components are only visible in higher order correlation functions like  $g^{(2)}$ . This also means that quantum jumps have a negligible effect on the system dynamics, and they were neglected in the calculations. In more general circumstances, using MPS simulations, we will show that the effects of quantum jumps and pulse distortion can have a significant effect on the output field.

For concreteness, we take input pulses with central frequency  $\omega_p$  and Gaussian envelope  $\mathcal{E}_{\text{in}}(t) = \alpha(\pi\sigma_t^2/2)^{-1/4} \exp(-(t-T)^2/\sigma_t^2)$ , which have an average photon number of  $\langle n_{\text{pulse}} \rangle = |\alpha|^2 \sim 1$ . The average photon number chosen is not due to any intrinsic limitation coming from the MPS method itself, but rather because in VIT the spatial separation is largest for the Fock components with low photon number (see Fig. 3(c)) and with  $|\alpha|^2 = 1$  the single photon and two photon components of the coherent state give an equal contribution to intensity emphasizing this effect. In this case number states with three or more photons make up 8% of the input state and constitute 26% of the input intensity due to their high photon number.

In the case of VIT, the atomic part  $H_0$  of the total Hamiltonian of Eq. (9) is given by

$$H_0 = - \sum_j \left( \Delta + i \frac{\Gamma'}{2} \right) \sigma_{ee}^j - \left( \delta_c + i \frac{\kappa}{2} \right) a^\dagger a + g \sum_j (\sigma_{es}^j a + \text{h.c.}). \quad (12)$$

Here  $\delta_c = \omega_p - \omega_c - \omega_{sg}$  is the VIT two-photon detuning and  $\kappa$  is the decay rate of the cavity mode. In what follows we assume both the probe and cavity are resonant with their respective transitions, so that  $\Delta = \delta_c = 0$ . The jump operator corresponding to this cavity decay is  $O_c = \sqrt{\kappa}a$  and we assume that the atomic excited state can decay via free-space spontaneous emission into either state  $|g\rangle$  or  $|s\rangle$  (taking these decay rates to be equal for simplicity), leading to  $2N$  jump operators  $O_{j,ge} = \sqrt{\Gamma'/2}\sigma_{ge}^j$  and  $O_{j,se} = \sqrt{\Gamma'/2}\sigma_{se}^j$ . The collective jump operators  $O_{R,L}$  corresponding to the emission of a photon in the forward or backward direction are as described in Section II. The cavity mode is represented in our MPS treatment by an additional site in our spin chain, which can support up to  $n_c$  bosonic excitations. In the simulations we present here we have taken  $n_c = 10$  and observe no difference in observables if  $n_c$  is increased.

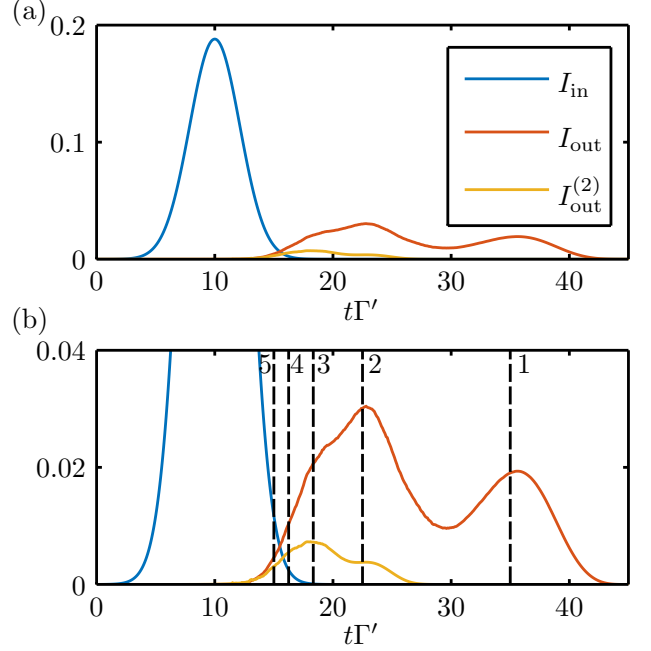


FIG. 4. (a) Pulse propagation in a VIT medium with optical depth  $OD = 400$ , simulated using  $N = 100$  atoms coupled to a 1D-waveguide, and averaged over 20000 quantum trajectories. Input of a coherent pulse with  $|\alpha|^2 = 1$  (blue) results in an output intensity  $I_{\text{out}}(t)$  (red) with two main peaks. Also plotted is the second-order correlation function  $I_{\text{out}}^{(2)}(t, t)$  (yellow). (b) Zoom of the plot above, with dashed lines showing the expected positions of pulses delayed by  $\tau_n$ , for  $n = 1, \dots, 5$ . Simulation parameters are  $\Gamma' = 1$ ,  $\Gamma_{1D} = 2$ ,  $\Delta = \delta_c = 0$ ,  $g = 2$ ,  $\kappa = 0.03$ ,  $\sigma_t = 3$  and  $T = 10$ . We chose  $D = 50$  and  $\delta t = 0.01$  where convergence was observed for all observables of interest (see Appendix B).

In Fig. 4(a)-(b) we show the time-dependent output pulse intensity  $I_{\text{out}}(t) = \langle E_{\text{out}}^\dagger(t) E_{\text{out}}(t) \rangle$  calculated using the input-output relation Eq. (8) from an MPS simulation of 100 atoms and an input pulse with  $|\alpha|^2 = 1$ . We also show the zero-delay second order correlation function  $I_{\text{out}}^{(2)}(t, t) = \langle E_{\text{out}}^\dagger(t) E_{\text{out}}^\dagger(t) E_{\text{out}}(t) E_{\text{out}}(t) \rangle$ . In the output intensity two main peaks are observed, where the first peak in time ( $t\Gamma' \sim 23$ ) is due to photon number components with two or more photons, while the last peak ( $t\Gamma' \sim 36$ ) is associated with the slow propagation and exit of the single-photon component. That the most delayed part contains only single photons can be seen by looking at the second order correlation function which is only non-zero in the first part of the pulse. In Fig. 4(b) we see good agreement of the features of the numerical pulse shape with the expected group velocity for each part of the pulse (compare with Fig. 3(c)), where the vertical black dashed lines represent the expected times for the peaks of the Fock state components, that is, with delays  $\tau_n$ .

Compared with the ideal picture in Fig. 3(c), where a



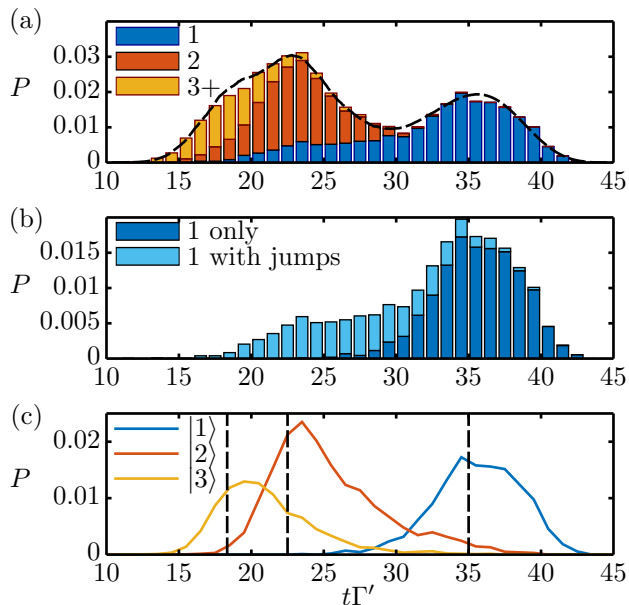


FIG. 5. (a) Stacked bar graph of quantum jumps into the output channel over the 20000 quantum trajectories used in Fig. 4. The height of each bar is the proportion  $P$  of trajectories that have an output channel jump occurring in the time bin defined by the bars width. The bars are then divided into three categories by classifying each jump according to how many jumps into the output channel occur for a particular trajectory (1, 2, or 3 or more). Jumps from trajectories where there are a higher number of photons emitted into the output channel are seen to occur earlier. For comparison the dashed black line shows the output intensity from Fig. 4. (b) Stacked bar graph for quantum jumps from trajectories where only a single photon is detected in the output of the waveguide. These jumps are then divided into jumps that are not accompanied by any other jump into other channels, and those that are. We see that the tail of photons detected earlier are due to trajectories where 2 or more photons propagated together but all but one were lost into other channels. (c) Post-selection of trajectories to find evolution for Fock state input. By selecting only trajectories where there were a total of 1 (blue), 2 (red), or 3 (yellow) jumps into any channel we can reconstruct the intensity output for the corresponding input Fock state.

clean separation is seen between one and two photons, one can see that the full simulation produces a much larger intensity between the one- and two-photon peaks. We now show how the trajectories from the MPS simulations can be further filtered and analyzed, to gain insight about the underlying physics. In particular, we find that quantum jumps play a key role in blurring the separation between the different number components in the output, even for the very good system parameters that we have chosen ( $\text{OD} = 400$ ,  $g/\kappa \sim 70$ ). An intuitive picture of how the blurring occurs can be gained by considering two photons that enter the medium, and initially propagate at a velocity  $v_2 = 2v_1$ . During evolution, this state may decay via spontaneous emission into free space into

a single propagating photon, at which point the group velocity is slowed to  $v_1$ . This change in group velocity can happen at any point in the system and leads to single photons that arrive at the output earlier than expected if just a single-photon Fock state was input into the system, destroying the perfect separation of the single photon output from the two photon component.

We can quantify this behavior by analyzing the quantum jumps that happen in our simulations, where due to the choice of physical jump operators discussed in Section III, the total number of jumps in a given trajectory corresponds to the number of photons emitted from the system. Furthermore, the type of jumps (and thus the emission channel) can be explicitly tracked, between free-space loss, cavity loss, or detection in the waveguide output. In Fig. 5(a), we create a histogram of jumps corresponding to output into the waveguide versus time for the 20000 trajectories used to produce Fig. 4. The count of the jumps in the output channel provides an alternative way (compare to Fig. 4) to calculate the intensity, as would be done in an experiment where detector counts are summed over many identical realizations. In Fig. 5(a), the vertical axis is re-scaled in units of intensity rather than total number of events, to yield a more direct comparison with the previously calculated output intensity (black dotted line).

Furthermore, we can classify the jumps according to whether they come from trajectories where 1, 2 or 3+ photons are emitted into the waveguide (as indicated by the different bar colors in Fig. 5(a)). As we see in the plot, the higher the number detected in the waveguide, the earlier in time the jumps happen, in agreement with the the simple theoretical model and with the calculations of  $I_{\text{out}}(t)$  and  $I_{\text{out}}^{(2)}(t, t)$ , discussed above. We can also select only the trajectories where a single photon is detected at the waveguide output, and further separate those trajectories into two distinct cases: (i) when that is the only jump event (indicating a single photon was input and successfully propagated through the system), and (ii) where a multi-photon state was input, and all but one photon decayed into other channels. The histogram according to this classification in time is shown in Fig. 5(b), where we see that the tail of faster arriving single photons, seen to the left of the main peak, results from the decay of number states with two or more photons, and the resulting mixing of propagation velocities.

Alternatively, we can use the jump statistics from a coherent state input to identify the intensity resulting from a Fock state input. Since the VIT system does not support any long lived excitations (compared with the simulated time scale), the total number of photon jumps (into any channel) out of the system for any one trajectory is equal to the number of the photons that entered the system for that trajectory. By post-selection on the total number of jumps we can then find the intensity that results from a Fock state input as shown in Fig. 5(c). Here we see the same effect of jumps as noted above but observed in a different way. In particular, while we cat-

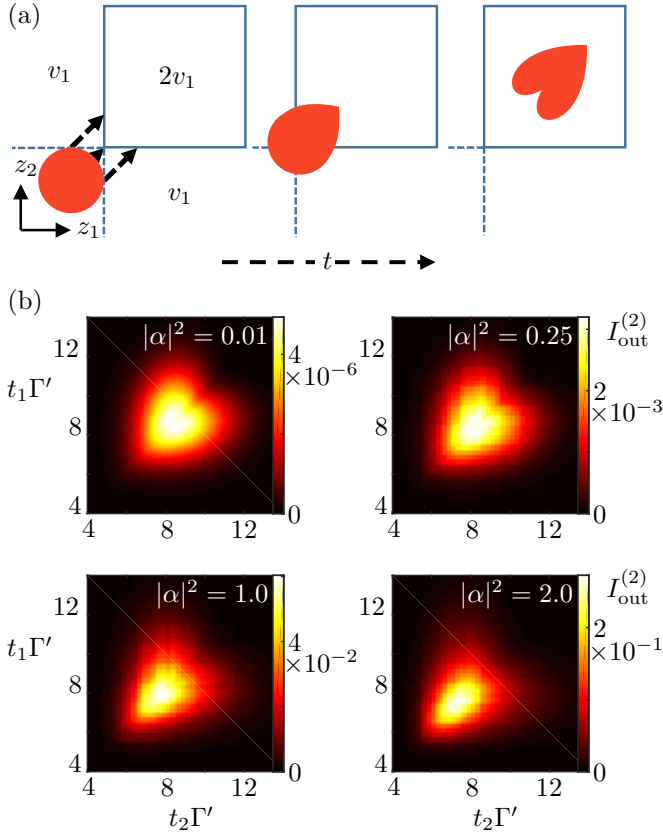


FIG. 6. (a) Illustration of pulse distortion as a two-photon wave-function  $\psi(z_1, z_2)$  enters the atomic medium. The initial Gaussian distribution of the photon positions  $z_1$  and  $z_2$  is shown as a circle. We can then divide the two-dimensional space of the photon pair into regions where only one photon is inside the medium and has group velocity  $v_1$ , indicated by the dashed lines, and when both photons are inside the medium having velocity  $v_2 = 2v_1$ , the square box. Photon pairs with greater separation spend more time in the regions where only one photon is inside the medium, delaying them compared to pairs with  $z_1 = z_2$ , leading to a characteristic heart shaped pattern. (b) Two-time correlation function for the output field,  $I_{\text{out}}^{(2)}(t_1, t_2)$ , of the VIT system, after excitation with a coherent Gaussian input pulse for various average input photon number,  $|\alpha|^2 = 0.01, 0.25, 1.0$  and  $2.0$ . At weak input field the two-time correlation function is purely due to the two photon component and shows a clean heart shape. As the number of input photons increases, higher photon number components contribute, which travel faster through the medium distorting the pattern and pulling it forward in time. The system parameters were for an optical depth of  $\text{OD} = 60$ , with  $N = 30$ ,  $\Gamma' = 1$ ,  $\Gamma_{1D} = 1$ ,  $\Delta = \delta_c = 0$ ,  $g = 2$ ,  $\kappa = 0.03$ ,  $\sigma_t = 4$  and  $T = 6$ . We chose a bond dimension of  $D = 30$  and a time step of  $\delta t = 0.01$  where convergence was observed for all observables of interest (Appendix B).

egorized the trajectories in Fig. 5(a),(b) by the number of photons that survive and are output, in Fig. 5(c) we classify them by the number that are input. For Fock state inputs of two or more photons, the output intensities show tails of longer than expected delay times, again as a result of photon loss and the mixing of propagation

speeds.

These longer than expected delay times are not only due to quantum jumps however, they can also result from distortion of the multi-photon wavepacket as it enters the medium [23]. This distortion happens as the input pulse crosses the boundary of the atomic ensemble, as we illustrate for a two-photon wave function in Fig. 6(a). For example, if the two photon wave function has a Gaussian pulse shape, the two photons can arrive at the boundary of the atomic ensemble at different times. The first photon that enters then travels at  $v_1$  until the time that the second photon enters and the group velocity becomes  $2v_1$ . A similar process occurs when the photons exit the medium. In this case the further the photons are separated in the original pulse, the larger the delay of the photons. This process distorts the two-photon input Gaussian into a heart shaped output and higher photon number manifolds into higher dimensional hearts. In Fig. 6(b) we show how this behavior can be observed in the two time correlation measurement of the output photons for an input coherent pulse at low input photon number. For higher photon number input the heart shape is distorted as higher photon number manifolds with larger group velocity smear out the distribution.

## V. DISCUSSION

In summary, we have described a novel technique to numerically simulate quasi-1D quantum light propagation through atomic ensembles, which is based on the powerful toolbox of matrix product states. This technique appears quite versatile, and adaptable to many cases of theoretical and experimental interest (e.g., with regard to level structure, types of interactions, additional degrees of freedom, etc.). Similar to the important role that DMRG and MPS played in one-dimensional condensed matter systems, we envision that results gained from our numerical techniques could be used to push forward the development of effective theories of strongly interacting systems of light [11, 12, 17–21], and conversely that such analytical work could be used to improve numerical algorithms.

Beyond that, it would be also interesting to investigate further why MPS apparently works well in the context of our open, long-range interacting system, and under what conditions MPS might fail. This could help to provide insight into the growth of entanglement, which naively seems like a potentially useful resource, but which has not been explored for such systems to our knowledge. Finally, the ability to formally map atom-light interactions to a quantum spin model appears rather intriguing in general, and it would be interesting to explore whether other techniques for solving spin systems could be applied here as well.

## VI. ACKNOWLEDGEMENTS

The authors thank J. J. Garcia-Ripoll and L. Mathey for stimulating discussions. This work was supported by Fundacio Privada Cellex Barcelona, the MINECO Ramon y Cajal Program, MINECO Severo Ochoa Grant No. SEV-2015-0522, MINECO Plan Nacional Grant CANS, Marie Curie Career Integration Grant ATOMNANO, ERC Starting Grant FoQAL, the European Commission FET Open XTrack Project GRASP and la Caixa-Severo Ochoa PhD Fellowship.

### Appendix A: Matrix product operators

Here we present the matrix product operators of the effective Hamiltonian and the corresponding jump operators for the spin-model for the simple case of two-level atoms, followed by the extension to the VIT case. Following the prescription of Ref. [25], for example, the matrices  $W_i$  in the MPO representation of  $H_{\text{eff}} = W_1 W_2 \dots W_N$ , are

$$W_j = \begin{pmatrix} \mathcal{I}^j & -\frac{i\lambda\Gamma_{1D}}{2} \sigma_{ge}^j & -\frac{i\lambda\Gamma_{1D}}{2} \sigma_{ge}^j & H_{\text{loc}}^j \\ 0 & \lambda \mathcal{I}^j & 0 & \sigma_{ge}^j \\ 0 & 0 & \lambda \mathcal{I}^j & \sigma_{eg}^j \\ 0 & 0 & 0 & \mathcal{I}^j \end{pmatrix}, \quad (\text{A1})$$

for  $1 < j < N$ , and

$$W_1 = \left( \mathcal{I}^1 \quad -\frac{i\lambda\Gamma_{1D}}{2} \sigma_{eg}^1 \quad -\frac{i\lambda\Gamma_{1D}}{2} \sigma_{ge}^1 \quad H_{\text{loc}}^1 \right), \quad (\text{A2})$$

$$W_N = \left( H_{\text{loc}}^N \quad \sigma_{ge}^N \quad \sigma_{eg}^N \quad \mathcal{I}^N \right)^T, \quad (\text{A3})$$

where  $\lambda = e^{ik_{\text{in}}d}$  and  $H_{\text{loc}}$  contains all the local terms in  $H_{\text{eff}}$ . The MPO of the linear expansion of the time evolution operator  $\mathcal{I} - i\delta t H_{\text{eff}}$  can be obtained from this MPO without increasing the bond dimension. It is enough to replace  $W_1$  with

$$W_1^{\text{t.e.}} = \left( -i\delta t \mathcal{I}^1 \quad -\frac{\delta t \lambda \Gamma_{1D}}{2} \sigma_{eg}^1 \quad -\frac{\delta t \lambda \Gamma_{1D}}{2} \sigma_{ge}^1 \quad -i\delta t H_{\text{loc}}^1 + \mathcal{I}^1 \right), \quad (\text{A4})$$

to obtain the desired MPO.

The jump operator corresponding to the emission of a photon in the right output channel can be written as  $O_R = Z_1 Z_2 \dots Z_N$  with

$$Z_j = \begin{pmatrix} \mathcal{I}^j & -i\sqrt{\Gamma_{1D}/2} e^{-ik_{\text{in}}z_j} \sigma_{ge}^j \\ 0 & \mathcal{I}^j \end{pmatrix}, \quad (\text{A5})$$

for  $1 < j < N$ , and

$$Z_1 = \left( \mathcal{I}^1 \quad -i\sqrt{\Gamma_{1D}/2} e^{-ik_{\text{in}}z_1} \sigma_{ge}^1 + \mathcal{E}(t) \mathcal{I}^1 \right), \quad (\text{A6})$$

$$Z_N = \left( -i\sqrt{\Gamma_{1D}/2} e^{-ik_{\text{in}}z_N} \sigma_{ge}^N \quad \mathcal{I}^N \right)^T. \quad (\text{A7})$$

The MPO of  $O_L$  is analogous, but without the external field term in  $Z_1$  and with  $k_{\text{in}}$  replaced by  $-k_{\text{in}}$ . For the jumps associated with spontaneous emission into free space an MPO representation is not required as these jumps just require an operator to be applied locally to a single site.

The MPO of the VIT Hamiltonian can be obtained by extending the bare spin model case above. The cavity degree of freedom is associated with an additional site in the spin chain at position  $N+1$ , in which case the VIT MPO of  $H_{\text{eff}}$  is obtained by adding two columns and rows to the bare representation:

$$W_j^{\text{VIT}} = \begin{pmatrix} \dots & \dots & \dots & g\sigma_{es}^j & g\sigma_{se}^j & \dots \\ \dots & \dots & \dots & 0 & 0 & \dots \\ \dots & \dots & \dots & 0 & 0 & \dots \\ 0 & 0 & 0 & \mathcal{I}^j & 0 & 0 \\ 0 & 0 & 0 & 0 & \mathcal{I}^j & 0 \\ \dots & \dots & \dots & 0 & 0 & \dots \end{pmatrix}, \quad (\text{A8})$$

for  $1 < j \leq N$ , where the dots stand for the elements given in Eq. (A1) and

$$W_{N+1}^{\text{VIT}} = \left( H_{\text{loc,cav}} \quad 0 \quad 0 \quad a \quad a^\dagger \quad \mathcal{I}^{\text{cav}} \right)^T. \quad (\text{A9})$$

### Appendix B: Convergence of the algorithm

In this appendix we discuss the convergence of the algorithm introduced. As discussed in the main text, within the MPS ansatz the “true” state of the system is approximated by a state belonging to the MPS family characterized by the maximum bond dimension  $D$ . If one considers a larger family of dimension  $D' > D$  and the values of observables of interest do not change, then we can say that the family of MPS characterized by  $D$  represent well the state of the system. In Fig. 7(a),(b) we plot the output intensity and zero-delay second-order correlation function for different bond dimensions for the trajectory without jumps (similar results hold for the other trajectories). We see that the intensity has an excellent convergence already for  $D = 20$ , while the zero-delay second-order correlation function converges for  $D = 40$ , except for the part of the pulse corresponding to high photon numbers. In our simulations thus we fix the bond dimension to the value of  $D = 50$ .

As discussed in the main text, time evolving an MPS increases its dimensions exponentially as a function of the number of time steps. To keep the size of the MPS manageable it is thus necessary to compress the MPS after making a time step from one with large maximum bond dimension  $D'$  to a smaller dimension  $D$ . Moreover, this compression must be done in a controlled fashion such that the error incurred is minimal. This compression can be done variationally minimizing the distance between  $|\psi(t)\rangle_D$  and  $|\psi(t)\rangle_{D'}$ , or by a sequence of singular value decompositions (SVD) of the bond connections between each site [25]. In the later case, if we denote by  $\lambda_{t,j,l}$  the set of singular values at bond site  $j$  and time  $t$ , with

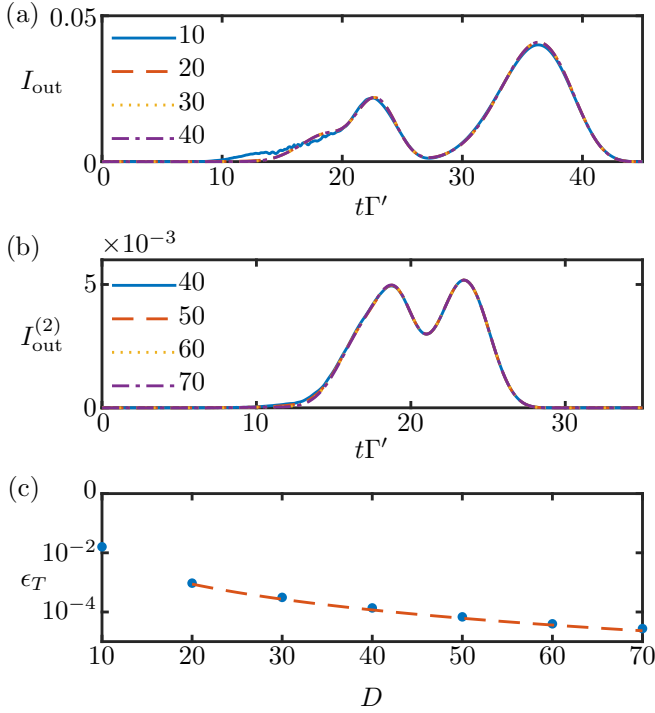


FIG. 7. (a) Intensity and (b) zero-delay second-order correlation function along the quantum trajectory without jumps for different values of the maximum bond dimension  $D$ . (c) Log-scale accumulated compression error  $\epsilon_T$  as function of the MPS maximum bond dimension  $D$  (blue dots). The red line is a polynomial fit,  $\epsilon_T \propto D^{-2.9}$ , for all the points except  $D = 10$ .

$1 \leq l \leq D'$  (with the singular values ordered to monotonically decrease with increasing  $l$ ), then we may reduce the bond dimension by only keeping the singular values with  $l \leq D$ . One measure of this compression error is the norm of the difference of the original state and the compressed state  $\epsilon_t = \|\psi(t)\rangle_D - |\psi(t)\rangle_{D'}\|$ , which can be expressed as  $\epsilon_t = 1 - \prod_{j=1}^{N-1} (1 - \epsilon_{t,j})$  with  $\epsilon_{t,j} = \sum_{l>D} \lambda_{t,j,l}^2$ . The error accumulated during the whole time evolution is  $\epsilon_T = 1 - \prod_t (1 - \epsilon_t)$ . Since all the terms are small one can approximate the products with sums and obtain

$$\epsilon_T \approx \sum_{t=0}^{T_f} \sum_{j=1}^{N-1} \sum_{l>D} \lambda_{t,j,l}^2. \quad (\text{B1})$$

$\epsilon_T$  is a figure of merit for the quality of the time evolution. In Fig. 7(c) we plot the accumulated error for different bond dimensions. We find that starting from  $D = 20$  the accumulated error decays as a power law  $\epsilon_T \sim D^{-\alpha}$ , with  $\alpha \approx 2.9$ , indicating a polynomial decay of the singular values  $\lambda_l \sim l^{-2}$ .

- 
- [1] M. Fleischhauer, A. Imamoglu, and J. P. Marangos, *Rev. Mod. Phys.* **77**, 633 (2005).
  - [2] K. Hammerer, A. S. Sørensen, and E. S. Polzik, *Rev. Mod. Phys.* **82**, 1041 (2010).
  - [3] T. Peyronel, O. Firstenberg, Q.-Y. Liang, S. Hofferberth, A. V. Gorshkov, T. Pohl, M. D. Lukin, and V. Vuletic, *Nature* **488**, 57 (2012).
  - [4] O. Firstenberg, T. Peyronel, Q.-Y. Liang, A. V. Gorshkov, M. D. Lukin, and V. Vuletic, *Nature* **502**, 71 (2013).
  - [5] J. D. Pritchard, K. J. Weatherill, and C. S. Adams, “Nonlinear Optics Using Cold Rydberg Atoms,” in *Annual Review of Cold Atoms and Molecules, Volume 1.*, edited by K. Madison, Y. Wang, and A. M. Rey (World Scientific Publishing Co, 2013) pp. 301–350.
  - [6] C. Murray and T. Pohl, “Quantum and nonlinear optics in strongly interacting atomic ensembles,” in *Advances In Atomic, Molecular, and Optical Physics*, Vol. 65, edited by C. C. L. Ennio Arimondo and S. F. Yelin (Academic Press, 2016) pp. 321 – 372.
  - [7] O. Firstenberg, C. S. Adams, and S. Hofferberth, *Journal of Physics B: Atomic, Molecular and Optical Physics* **49**, 152003 (2016).
  - [8] A. Goban, C.-L. Hung, S.-P. Yu, J. Hood, J. Muniz, J. Lee, M. Martin, A. McClung, K. Choi, D. Chang, O. Painter, and H. Kimble, *Nat. Commun.* **5**, 3808 (2014).
  - [9] J. D. Hood, A. Goban, A. Asenjo-Garcia, M. Lu, S.-P. Yu, D. E. Chang, and H. J. Kimble, *Proc. Natl. Acad. Sci. USA* **113**, 10507 (2016).
  - [10] J. S. Douglas, H. Habibian, C.-L. Hung, A. V. Gorshkov, H. J. Kimble, and D. E. Chang, *Nat. Photon.* **9**, 326 (2015).
  - [11] E. Shahmoon, P. Grišins, H. P. Stimming, I. Mazets, and G. Kurizki, *Optica* **3**, 725 (2016).
  - [12] J. S. Douglas, T. Caneva, and D. E. Chang, *Phys. Rev. X* **6**, 031017 (2016).
  - [13] E. Vetsch, D. Reitz, G. Sagué, R. Schmidt, S. T. Dawkins, and A. Rauschenbeutel, *Phys. Rev. Lett.* **104**, 203603 (2010).
  - [14] C. Lang, D. Bozyigit, C. Eichler, L. Steffen, J. M. Fink, A. A. Abdumalikov, M. Baur, S. Filipp, M. P. da Silva, A. Blais, and A. Wallraff, *Phys. Rev. Lett.* **106**, 243601 (2011).
  - [15] I.-C. Hoi, C. M. Wilson, G. Johansson, T. Palomaki, B. Peropadre, and P. Delsing, *Phys. Rev. Lett.* **107**, 073601 (2011).
  - [16] Y. Liu and A. A. Houck, *Nat Phys* **13**, 48 (2017).
  - [17] J. Otterbach, M. Moos, D. Muth, and M. Fleischhauer, *Phys. Rev. Lett.* **111**, 113001 (2013).

- [18] M. F. Maghrebi, M. J. Gullans, P. Bienias, S. Choi, I. Martin, O. Firstenberg, M. D. Lukin, H. P. Büchler, and A. V. Gorshkov, *Phys. Rev. Lett.* **115**, 123601 (2015).
- [19] M. F. Maghrebi, N. Y. Yao, M. Hafezi, T. Pohl, O. Firstenberg, and A. V. Gorshkov, *Phys. Rev. A* **91**, 033838 (2015).
- [20] M. J. Gullans, J. D. Thompson, Y. Wang, Q.-Y. Liang, V. Vuletić, M. D. Lukin, and A. V. Gorshkov, *Phys. Rev. Lett.* **117**, 113601 (2016).
- [21] E. Zeuthen, M. J. Gullans, M. F. Maghrebi, and A. V. Gorshkov, *arXiv preprint arXiv:1608.06068* (2016).
- [22] A. V. Gorshkov, J. Otterbach, M. Fleischhauer, T. Pohl, and M. D. Lukin, *Phys. Rev. Lett.* **107**, 133602 (2011).
- [23] N. Lauk and M. Fleischhauer, *Phys. Rev. A* **93**, 063818 (2016).
- [24] F. Verstraete, V. Murg, and J. Cirac, *Advances in Physics* **57**, 143 (2008).
- [25] U. Schollwöck, *Annals of Physics* **326**, 96 (2011).
- [26] T. Caneva, M. T. Manzoni, T. Shi, J. S. Douglas, J. I. Cirac, and D. E. Chang, *New Journal of Physics* **17**, 113001 (2015).
- [27] S. Xu and S. Fan, *Phys. Rev. A* **91**, 043845 (2015).
- [28] K. Lalumière, B. C. Sanders, A. F. van Loo, A. Fedorov, A. Wallraff, and A. Blais, *Phys. Rev. A* **88**, 043806 (2013).
- [29] A. Asenjo-Garcia, J. Hood, D. Chang, and H. Kimble, *arXiv preprint arXiv:1606.04977* (2016).
- [30] A. Goban, C.-L. Hung, J. D. Hood, S.-P. Yu, J. A. Muniz, O. Painter, and H. J. Kimble, *Phys. Rev. Lett.* **115**, 063601 (2015).
- [31] J. E. Field, *Phys. Rev. A* **47**, 5064 (1993).
- [32] H. Tanji-Suzuki, W. Chen, R. Landig, J. Simon, and V. Vuletić, *Science* **333**, 1266 (2011).
- [33] G. Nikoghosyan and M. Fleischhauer, *Phys. Rev. Lett.* **105**, 013601 (2010).
- [34] H. T. Dung, L. Knöll, and D.-G. Welsch, *Phys. Rev. A* **66**, 063810 (2002).
- [35] S. Y. Buhmann and D.-G. Welsch, *Progress in Quantum Electronics* **31**, 51 (2007).
- [36] B. R. Mollow, *Phys. Rev. A* **12**, 1919 (1975).
- [37] A. F. Molisch and B. P. Oehry, *Radiation Trapping in Atomic Vapours* (Clarendon Press, 1998).
- [38] N. J. Schilder, C. Sauvan, J.-P. Hugonin, S. Jennewein, Y. R. P. Sortais, A. Browaeys, and J.-J. Greffet, *Phys. Rev. A* **93**, 063835 (2016).
- [39] W. Guerin, M. O. Araújo, and R. Kaiser, *Phys. Rev. Lett.* **116**, 083601 (2016).
- [40] E. Zeuthen, A. Grodecka-Grad, and A. S. Sørensen, *Phys. Rev. A* **84**, 043838 (2011).
- [41] D. E. Chang, L. Jiang, A. V. Gorshkov, and H. J. Kimble, *New Journal of Physics* **14**, 063003 (2012).
- [42] D. E. Chang, A. S. Sørensen, E. A. Demler, and M. D. Lukin, *Nat Phys* **3**, 807 (2007).
- [43] J. T. Shen and S. Fan, *Opt. Lett.* **30**, 2001 (2005).
- [44] N. V. Corzo, B. Gouraud, A. Chandra, A. Goban, A. S. Sheremet, D. V. Kupriyanov, and J. Laurat, *Phys. Rev. Lett.* **117**, 133603 (2016).
- [45] H. L. Sørensen, J.-B. Béguin, K. W. Kluge, I. Iakoupov, A. S. Sørensen, J. H. Müller, E. S. Polzik, and J. Appel, *Phys. Rev. Lett.* **117**, 133604 (2016).
- [46] G. Birkel, M. Gatzke, I. H. Deutsch, S. L. Rolston, and W. D. Phillips, *Phys. Rev. Lett.* **75**, 2823 (1995).
- [47] M. Bajcsy, A. S. Zibrov, and M. D. Lukin, *Nature* **426**, 638 (2003).
- [48] M. Arcari, I. Söllner, A. Javadi, S. Lindskov Hansen, S. Mahmoodian, J. Liu, H. Thyrrstrup, E. H. Lee, J. D. Song, S. Stobbe, and P. Lodahl, *Phys. Rev. Lett.* **113**, 093603 (2014).
- [49] K. Mølmer, Y. Castin, and J. Dalibard, *J. Opt. Soc. Am. B* **10**, 524 (1993).
- [50] A. J. Daley, *Advances in Physics* **63**, 77 (2014).
- [51] F. Verstraete and J. I. Cirac, *Phys. Rev. B* **73**, 094423 (2006).
- [52] A. J. Daley, J. M. Taylor, S. Diehl, M. Baranov, and P. Zoller, *Phys. Rev. Lett.* **102**, 040402 (2009).
- [53] M. Zwolak and G. Vidal, *Phys. Rev. Lett.* **93**, 207205 (2004).
- [54] F. Verstraete, J. J. García-Ripoll, and J. I. Cirac, *Phys. Rev. Lett.* **93**, 207204 (2004).
- [55] J. Cui, J. I. Cirac, and M. C. Bañuls, *Phys. Rev. Lett.* **114**, 220601 (2015).
- [56] E. Mascarenhas, H. Flayac, and V. Savona, *Phys. Rev. A* **92**, 022116 (2015).
- [57] P. Rice and R. Brecha, *Optics Communications* **126**, 230 (1996).